Journal of
Mechanics of
Materials and Structures

STRAIN LOCALIZATION IN OPEN-CELL POLYURETHANE FOAMS: EXPERIMENTS AND THEORETICAL MODEL

Giampiero Pampolini and Gianpietro Del Piero

STRAIN LOCALIZATION IN OPEN-CELL POLYURETHANE FOAMS: EXPERIMENTS AND THEORETICAL MODEL

GIAMPIERO PAMPOLINI AND GIANPIETRO DEL PIERO

Confined compression tests performed by the authors on open-cell polyurethane foams reveal the presence of strain localization. After a brief description of the experiments, a theoretical model is proposed. In the model, the foam is represented as a chain of elastic springs with a two-phase strain energy density, and the strain localization is due to a progressive collapse of the springs. The collapse is a sort of continuum instability, which can be attributed to phase transition. An appropriate choice of the material constants leads to a close reproduction of the experimental force-elongation response curves.

1. Introduction

The rapidly increasing use of foam polymers, and of cellular materials in general, is due to a combination of some peculiar properties, such as lightness, easy packaging, and high energy absorption. Such properties come from the specific microstructure of the material, which consists of a complex network of ligaments and membranes. For a detailed description, see [Gibson and Ashby 1997]. Typical of such materials is the nonhomogeneous deformation exhibited in uniaxial compression tests. There is indeed experimental evidence that in a displacement-driven test the deformation is initially homogeneous, then localizes in transverse bands whose number grows with increasing deformation and eventually becomes again homogeneous, see, for example, [Lakes et al. 1993; Gioia et al. 2001; Wang and Cuitinho 2002; Gong and Kyriakides 2007], and the experiments made by the present authors described in the next section. This behavior determines a three-regime shape of the force-elongation response curve in which the central regime of strain localization corresponds to an almost horizontal plateau.

The same overall behavior was observed by Bart-Smith et al. [1998] and by Bastawros et al. [2000] in both open and closed-cell aluminium alloy foams. There is also a strong analogy with the response curves for shape memory alloy wires; see, for example, [Miyazaki and Otsuka 1989; Ortin 1992; Tanaka et al. 1996]. The analogy becomes even more interesting by the fact that for all such materials the loading-unloading tests exhibit hysteresis cycles of similar shapes [Tanaka et al. 1996; Bart-Smith et al. 1998; Bastawros et al. 2000; Gong et al. 2005].

To model the behavior of open-cell polymer foams, two main approaches are used: a numerical approach, directly reproducing the microstructure in the finite element scheme, and an analytical approach, based on the representation of the material as a continuum. In the numerical approach, the ligaments are usually represented as shear-deformable linear elastic beams, and strain localization is attributed to the buckling of the beams; see, for example, [Gent and Thomas 1963; Gibson and Ashby 1997; Warren and

Kraynik 1997]. In [Gong et al. 2005], the foam is modeled as a periodic structure whose basic element is a 14-sided polyhedron, called the Kelvin cell. In general, the numerical approach is computationally very demanding, due to the large number of unknowns and to difficulties in modeling the contact between beams in the post-buckling regime; see [Bardenhagen et al. 2005].

In the analytical approach, the material is considered to be a homogeneous hyperelastic continuum. Indeed, it was shown in [Ericksen 1975] that both strain localization and hysteretic behavior can be described within the elastic context, by assuming a nonconvex strain energy density of a special "double-well" shape. A model for foam polymers based on this simple idea was proposed in [Gioia et al. 2001].

In this paper we propose a discrete model whose origin traces back to a series of papers [Müller and Villaggio 1977; Fedelich and Zanzotto 1992; Puglisi and Truskinovsky 2000] in which Ericksen's problem is discretized by replacing a continuous bar by a finite chain of elastic springs with a double-well strain energy. The paper is divided into two parts. In the first part the test procedure and the experimental results are presented. In the second part the theoretical model is described and, by an appropriate identification of the constitutive constants, a close reproduction of the experimental force-elongation curves is obtained.

2. Experimental analysis

2.1. *Equipment and test procedure.* The compression tests were made using a load frame Instron 4467 with a 500 N load cell, located at the *Laboratorio di Materiali Polimerici* of the University of Ferrara. The specimens were parallelepipeds cut out from two sheets of commercial open-cell polyurethane foams, 10 and 50 mm thick, respectively. The cutting was done manually, using a ribbon saw. The cellular structures of the two sheets are shown in Figure 1, and their mass densities are 27 and 25 kg/m^3, respectively.

Ten specimens with base dimensions 100×100 mm, five for each of the thicknesses 10 and 50 mm, were tested in confined compression. Confinement was assured by a polystyrene box clamped to the load frame, of dimensions $101 \times 101 \times 60$ mm. The lower base of the samples was in contact with the bottom of the box, and the upper base was in contact with a steel plate fixed to the moving crosshead. Polystyrene,

(a)   (b)

1 mm
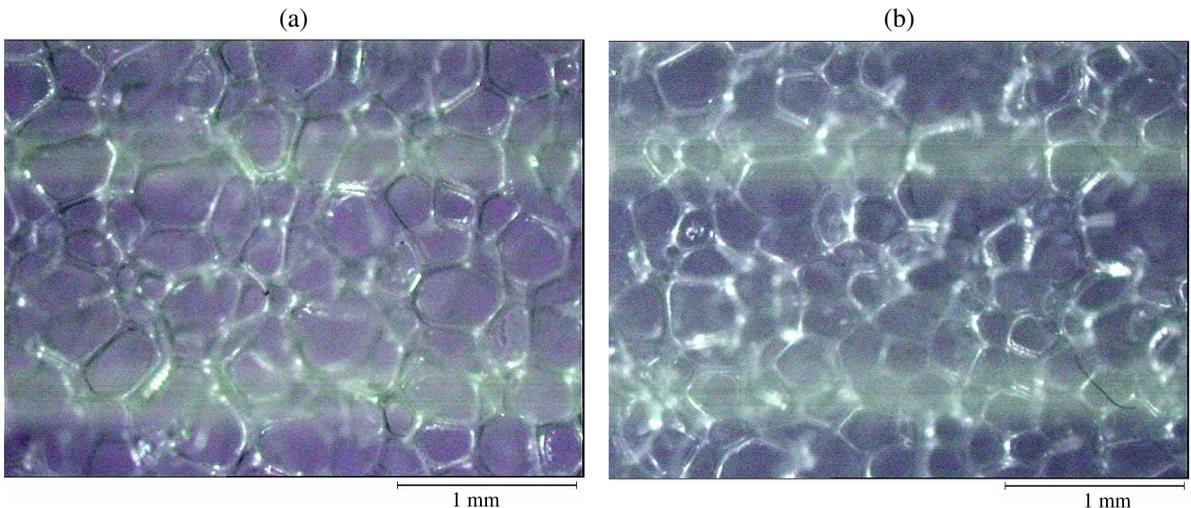
Figure 1. Cell structure of the polyurethane foams in the 50 mm (a) and 10 mm sheets (b).

Figure 2. The test equipment.

being transparent, allowed for optical control of the evolution of the deformation. Confinement was chosen to prevent lateral buckling, which was indeed observed in some collateral nonconfined tests. There were just slight differences between the response curves for confined and nonconfined tests. This led us to conclude that the effects of the friction between specimens and the lateral walls of the box were not important. Accordingly, we decided not to lubricate the walls of the box.

The testing equipment is shown in Figure 2. A preload of 2 to 3 N was applied to guarantee a full initial contact between plate and specimen. A crosshead speed of 1 mm/min was considered sufficiently slow to render negligible all rate-dependent effects. The test was stopped when the crosshead displacement reached 70 % of the specimen thickness, an elongation sufficient to capture all significant aspects of the force-elongation curve.

2.2. Results. Two experimental force-elongation curves are shown in Figure 3. They give the average responses of five tests made on 10 mm and 50 mm specimens, respectively. The figure shows the stress
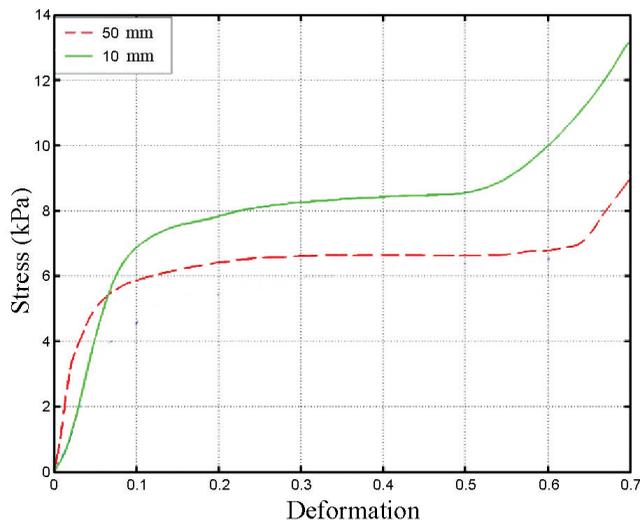
Figure 3. Comparison of the average force-elongation curves relative to five tests on 10 and 50 mm samples in confined compression.

(measured as axial force divided by the initial sample cross area) as a function of the deformation (measured as the crosshead displacement divided by the initial thickness of the specimen). The two curves are similar in shape. In particular, they exhibit the three-regime behavior mentioned in Section 1, characterized by a central plateau. The quantitative differences are significant. This means that the two commercial sheets from which the specimens were obtained have different mechanical properties. In the following, they will be considered as made of two different materials. From Figure 3, one sees that the initial slopes are about 110 and 145 kPa for the 10 mm and for the 50 mm specimens, respectively. The plateau occurs at a stress of about 6.5 kPa and 8.5 kPa, and ends at a deformation of about 55 % and 63 %, respectively.

To detect the strain localization, a rectangular grid was drawn on one of the specimens' sides. The progressive deformation of the grid under growing crosshead displacement is shown in Figure 4. As shown in Figure 4a, the deformation is initially homogeneous. Subsequently, a severe deformation occurs at the top layer of the specimen, Figure 4b. This deformation propagates to the underlying layers (Figures 4c, 4d), and after all layers have been reached, the deformation again becomes homogeneous, Figure 4e. The same qualitative evolution was observed in polyurethane low-density foams [Wang and Cuitinho 2002] and in aluminium alloy foams [Bart-Smith et al. 1998; Bastawros et al. 2000]. A very similar localization phenomenon was also observed in steel bars subjected to uniaxial tension [Froli and Royer-Carfagni 1997; 1999].
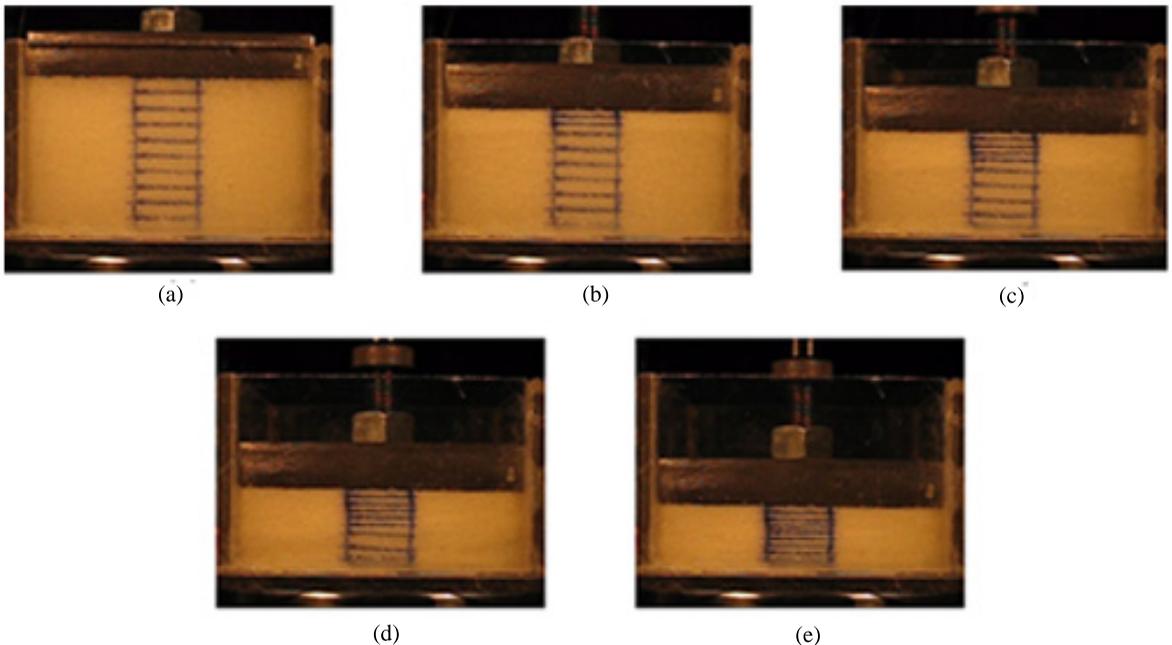
Figure 4. The deformation mechanism in confined compression test on the 50 mm thick samples: (a) the initial homogeneous deformation, (b) strain localization at the upper end of the specimen, (c) and (d) propagation to the underlying layers, and (e) the final homogeneous deformation. The initial equidistance of the horizontal lines of the rectangular grid is 5 mm.

In particular, Wang and Cuitinho [2002] observed the formation of three or four highly deformed bands orthogonal to the loading direction. In their experiments, localization does not initiate at the upper end of the specimen as in our tests. The fact that in our tests the localization systematically starts at the upper end can be explained by the difference in the contact conditions. Indeed, in collateral tests made with uniform contact conditions we observed that localization starts simultaneously at the two bases.

3. Theoretical model

3.1. *Basic ingredients.* Let Ω_0 be the bounded open three-dimensional region occupied by the body in the reference configuration, and let f be the deformation that maps the points X of Ω_0 into the points $x = f(X)$. Assume that the body is made of an isotropic hyperelastic material, with a strain energy density of the form

$$w(F) = \tfrac{1}{2} \alpha \, F \cdot F + \Gamma(\det F) , \tag{1}$$

where F denotes the gradient of f, α is a positive material constant, and Γ is a nonnegative function such that

$$\lim_{\det F \to 0} \Gamma(\det F) = \lim_{\det F \to +\infty} \Gamma(\det F) = +\infty. \tag{2}$$

The gradient of w,

$$S = w_F(F) = \alpha F + \det F \; \Gamma'(\det F) \, F^{-T}, \tag{3}$$

is the Piola–Kirchhoff stress tensor. If we take $w(I) = 0$ and if we assume that the reference configuration $F = I$ is stress-free, from the conditions $w(I) = w_F(I) = 0$ we get

$$\alpha = -\Gamma'(1) , \qquad \tfrac{3}{2} \alpha + \Gamma(1) = 0. \tag{4}$$

For the function Γ we assume the expression

$$\Gamma(\det F) = c \, (\det F)^n \left(\frac{1}{n+2} (\det F)^2 - \frac{1}{n} \right) - \mu \ln(\det F) + \frac{\beta \sqrt{\pi}}{2\sqrt{k}} \operatorname{erf}\left(\sqrt{k} \, (\det F - a) \right) + \gamma , \tag{5}$$

where $\alpha, c, n, \mu, \beta, k$ are positive constants, with $a \leqslant 1$, $\operatorname{erf}(\cdot)$ is the error function

$$\operatorname{erf}(x) = \frac{2}{\sqrt{\pi}} \int_0^x e^{-t^2} dt , \tag{6}$$

and γ is a constant determined by the conditions (4). The expression chosen for Γ is the sum of two parts. The first part, similar to the one proposed in [Ogden 1997], takes into account the long-range effects, while the second part, the error function, provides a local effect at values of $\det F$ close to a. In (5), the growth conditions of (2) are satisfied for any positive c, μ, and n. In the particular case of confined compression in the direction e, one has
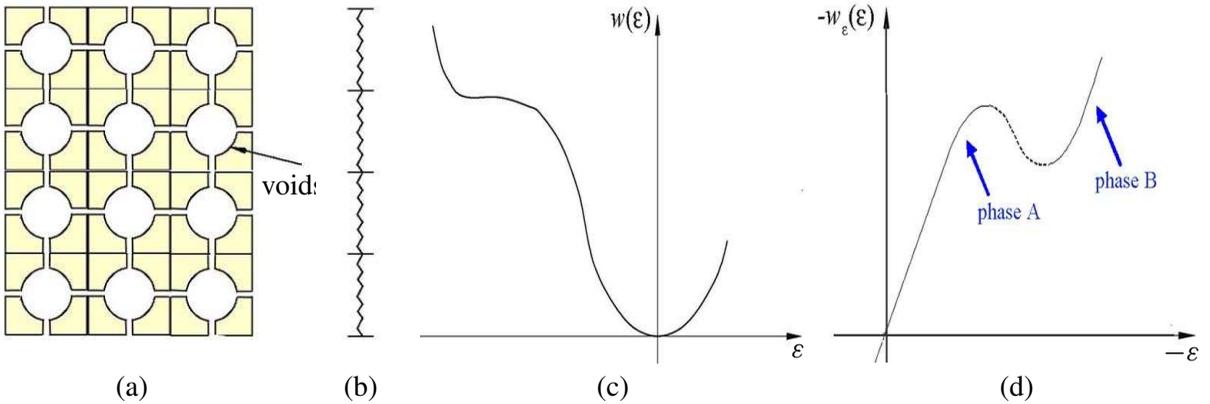
$$F = I + (\lambda - 1) e \otimes e , \qquad \det F = \lambda , \qquad 0 < \lambda < 1 , \tag{7}$$

so that

$$S = \left(\lambda \Gamma'(\lambda) - \Gamma'(1) \right) I + (1 - \lambda) \left(\Gamma'(\lambda) + \Gamma'(1) \right) e \otimes e. \tag{8}$$

We see that S depends only on λ and on the function Γ. The component of S in the loading direction is

$$\sigma = S \, e \cdot e = \Gamma'(\lambda) - \lambda \, \Gamma'(1). \tag{9}$$

Figure 5. Subdivision of the body into cell layers (a), representation of each layer as a nonlinear elastic spring (b) with nonconvex energy (c), and nonmonotonic force-elongation curve (d).

For Γ as in (5), Equation (9) yields

$$\sigma = \left[\mu - \beta \exp\left(-k(1-a)^2\right)\right]\lambda + c\lambda^{n-1}\left(\lambda^2 - 1\right) - \mu\lambda^{-1} + \beta \exp\left(-k(\lambda - a)^2\right). \tag{10}$$

This is the equation that, with appropriate identifications of the constants μ, β, k, a, c, n, will be used to reproduce the experimental curves.

To begin, consider (10) as the force-elongation relation (σ, λ) of a nonlinear elastic spring. This relation is represented by a curve in which two ascending branches are separated by a descending branch as shown in Figure 5d. It does not match with the curves in Figure 3 and, what is more, it does not provide any description of strain localization. But, as it will be shown in the coming subsection, both goals can be reached by assembling in series a sufficiently large number of such springs.

3.2. *The discrete model.* Consider a chain of n springs connected in series (Figure 5a) in which each spring represents a horizontal layer of cells as shown in Figure 5b. We assume that all springs have the nonconvex strain energy of the type shown in Figure 5c, to which corresponds the force-elongation law shown in Figure 5d and expressed by (10).

The total energy of the system is the sum of the strain energies of the springs,

$$E\left(\varepsilon_1, \varepsilon_2, \ldots, \varepsilon_n\right) = \sum_{i=1}^{n} w(\varepsilon_i), \tag{11}$$

where ε_i is the elongation of the ith spring. The chain is subjected to the *hard device* condition:

$$\sum_{i=1}^{n} \varepsilon_i = n\varepsilon_0, \tag{12}$$

where ε_0 is the prescribed average elongation of the springs. If one of the ends of the chain is fixed, the total elongation $n\varepsilon_0$ of the chain coincides with the displacement imposed on the other end. Using condition (12), one can eliminate one variable, say ε_n, and rewrite the energy in the form

$$E\left(\varepsilon_1, \varepsilon_2, \ldots, \varepsilon_{n-1}\right) = \sum_{i=1}^{n-1} w(\varepsilon_i) + w\left(n\varepsilon_0 - \sum_{i=1}^{n-1} \varepsilon_i\right). \tag{13}$$

In an elastic structure, the equilibrium configurations are identified with the stationarity points of the energy, and the stable equilibrium configurations are identified with the (local or global) energy minimizers. For the present structure, which has a finite number of degrees of freedom, the equilibrium configurations are found by annihilating the partial derivatives of the energy

$$\frac{\partial E}{\partial \varepsilon_i}\left(\varepsilon_1, \varepsilon_2, \ldots, \varepsilon_{n-1}\right) = w'(\varepsilon_i) - w'\left(n\varepsilon_0 - \sum_{j=1}^{n-1} \varepsilon_j\right) = 0, \quad i = 1, 2, \ldots, n-1. \tag{14}$$

Recalling that $\varepsilon_n = n\varepsilon_0 - \sum_{j=1}^{n-1} \varepsilon_j$, the above equality can be given the form

$$w'(\varepsilon_i) = w'(\varepsilon_n), \qquad i = 1, 2, \ldots, n-1, \tag{15}$$

which tells us that the force is the same in all springs. The common value of the force in the springs will be denoted by σ. As to the conditions for a global or local minimum, a sufficient condition is that the Hessian matrix of the second partial derivatives of the energy,

$$\frac{\partial^2 E}{\partial \varepsilon_i \, \partial \varepsilon_j} = \begin{cases} w''(\varepsilon_j) + w''(\varepsilon_n) & \text{if } i = j, \\ w''(\varepsilon_n) & \text{if } i \neq j. \end{cases} \tag{16}$$

be positive definite. After setting $A_i = w''(\varepsilon_i)$, this matrix takes the form

$$H = \begin{bmatrix} A_1 + A_n & A_n & . & A_n \\ A_n & A_2 + A_n & . & A_n \\ . & . & . & . \\ A_n & A_n & . & A_{n-1} + A_n \end{bmatrix}. \tag{17}$$

It is known (see, for example, [Puglisi and Truskinovsky 2000]) that H is positive definite if and only if (a) all A_i, except at most one, are positive, and (b) if there is a negative $A_j < 0$, it must be the case that

$$\sum_{i=1}^{n} A_i^{-1} < 0. \tag{18}$$

Condition (b) has no practical interest if n is sufficiently large; see [Puglisi and Truskinovsky 2000]. In what follows, we neglect it altogether. Because $A_i = w''(\varepsilon_i)$, a positive A_i means that the elongation ε_i lies on one of the two ascending branches of the force-elongation curve. Therefore, we confine ourselves to equilibrium configurations in which all elongations ε_i lie on one of the ascending branches. We say that the ith spring is in phase A if ε_i belongs to the first ascending branch, and that it is in phase B if ε_i belongs to the second ascending branch.

3.3. *Strain localization.* Consider an equilibrium configuration with m springs in phase A, for which the force $\bar{\sigma}$ belongs to the interval $(\sigma_{\min}, \sigma_{\max})$, where $\sigma_{\min}$ and $\sigma_{\max}$ are the local minimum and the local maximum of the force-elongation curve; see Figure 6a. Let us call $\bar{\varepsilon}_1$ and $\bar{\varepsilon}_2$ the elongations
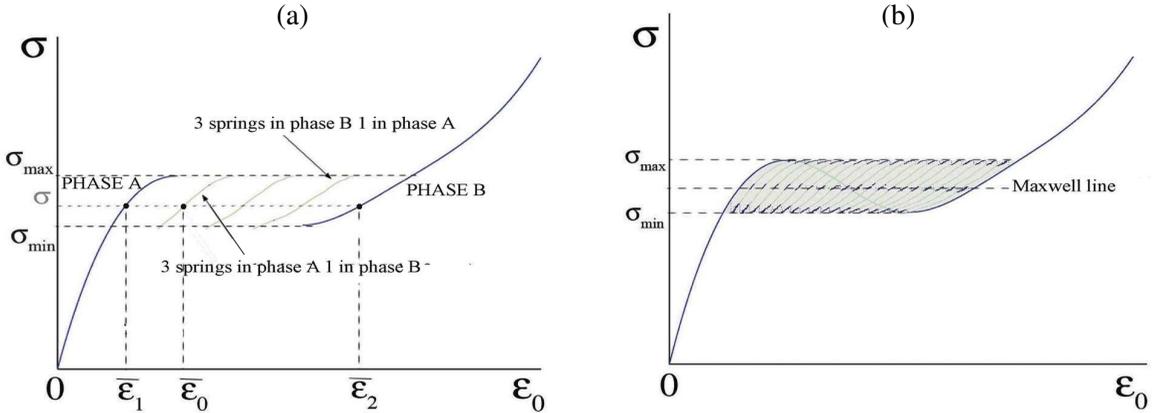
Figure 6. Response curves for (a) a system of 4 springs and (b) a system of 20 springs.

corresponding to $\bar{\sigma}$ in the first and second ascending branch, respectively. Then,
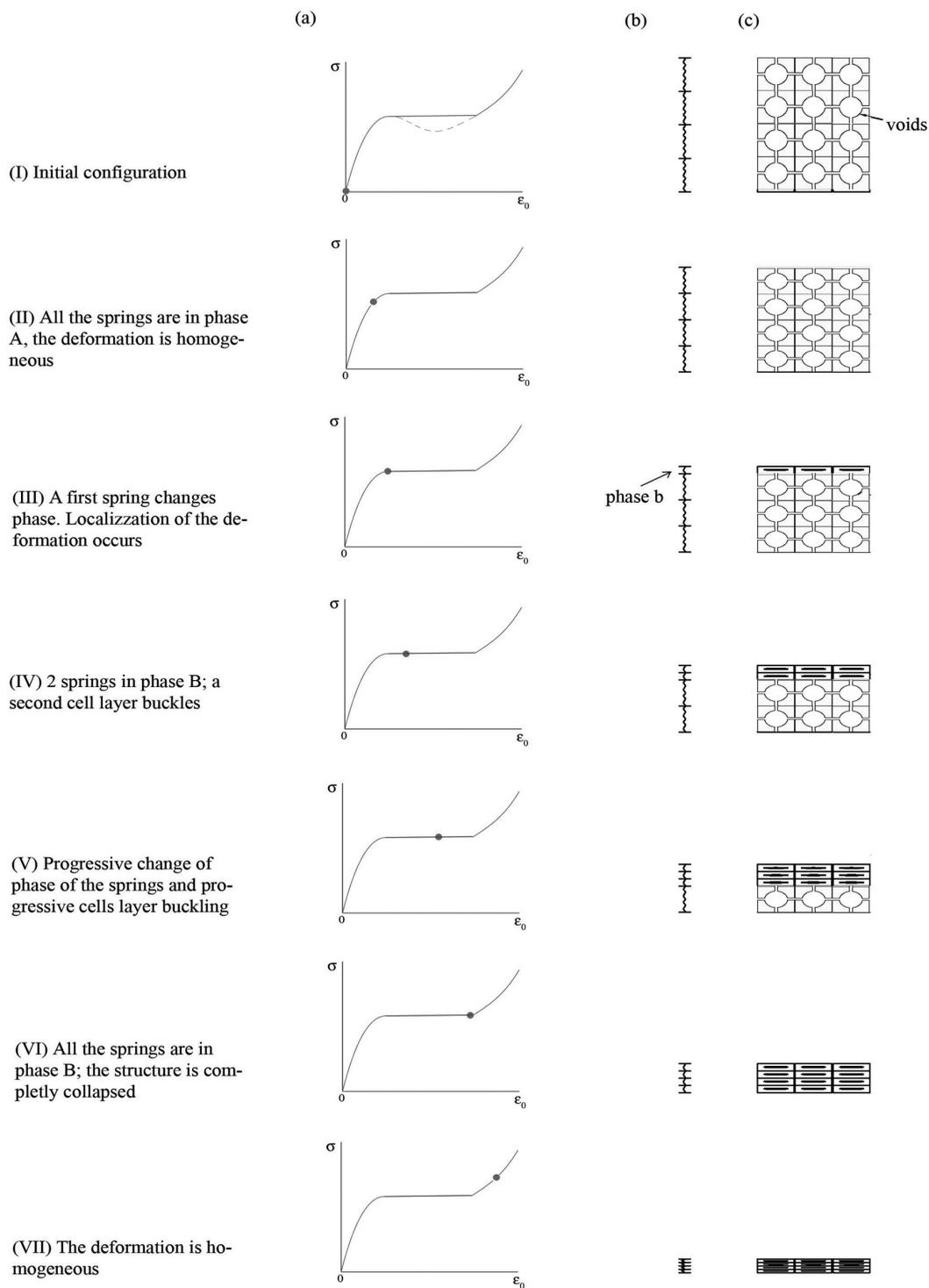
$$\bar{\varepsilon}_0 = \frac{m}{n} \, \bar{\varepsilon}_1 + \frac{n-m}{n} \, \bar{\varepsilon}_2 \tag{19}$$

is the corresponding average elongation. By varying $\bar{\sigma}$, for each fixed m one can construct the stable equilibrium path $(\bar{\sigma}, \bar{\varepsilon}_0)$, and by varying m one gets all equilibrium paths made of the equilibrium configurations selected above. In Figure 6a, the equilibrium paths for a system of four springs are shown.

The cases $m = 0$ and $m = n$ correspond to homogeneous configurations. Indeed, for $m = n$, from (19), we get $\bar{\varepsilon}_0 = \bar{\varepsilon}_1$, so that the path $(\bar{\sigma}, \bar{\varepsilon}_0)$ coincides with the first ascending branch. For $m = 0$ we get $\bar{\varepsilon}_0 = \bar{\varepsilon}_2$, so that the path $(\bar{\sigma}, \bar{\varepsilon}_0)$ coincides with the second ascending branch. If one assumes that the evolution occurs along equilibrium curves made of local energy minimizers (see [Del Piero and Truskinovsky $\geq$ 2008]) then the system, when loaded starting from the initial configuration, initially follows the first ascending branch, until the branch ends when the force reaches the value $\sigma_{\max}$.

At this point, to further increase ε_0, there are no more single-phase equilibrium configurations. It is reasonable to assume that the system jumps to the closest branch, which corresponds to the configurations with one spring in phase B and three springs in phase A. This phase transition requires a nonequilibrium process in which the force decreases at constant ε_0. This process will not be analyzed here. Once the new equilibrium branch has been reached, the force again increases, until σ reattains the value $\sigma_{\max}$. Then the system jumps to the branch with two springs in phase B and so on. When all springs have undergone the phase transition, the system evolves following the second ascending branch, which corresponds to single-phase configurations with all springs in phase B. Thus, after reaching the value $\sigma_{\max}$ for the first time, the system first follows a wavy, approximately horizontal line, successively assuming configurations with the number m of springs in phase A gradually decreasing from n to zero, and then follows the second ascending branch. By comparing the two halves of Figure 6, one sees that the number of intermediate branches, and therefore nonequilibrium processes, increases with n. At the same time, each phase transition involves a smaller jump of σ. Therefore the whole regime of progressive phase change occurs more smoothly.

Let us compare the model's predictions with the deformation mechanism observed in experiments. In Figure 7, the first row represents the undeformed configuration, and the second row shows the system

(a) (b) (c)

(I) Initial configuration

voids

(II) All the springs are in phase A, the deformation is homogeneous

(III) A first spring changes phase. Localizzation of the deformation occurs

phase b

(IV) 2 springs in phase B; a second cell layer buckles

(V) Progressive change of phase of the springs and progressive cells layer buckling

(VI) All the springs are in phase B; the structure is completly collapsed

(VII) The deformation is homogeneous

Figure 7. Description of the deformation mechanism following the response curve (a), and the corresponding configurations of the springs (b) and of the cell-layers (c).

(a)   (b)
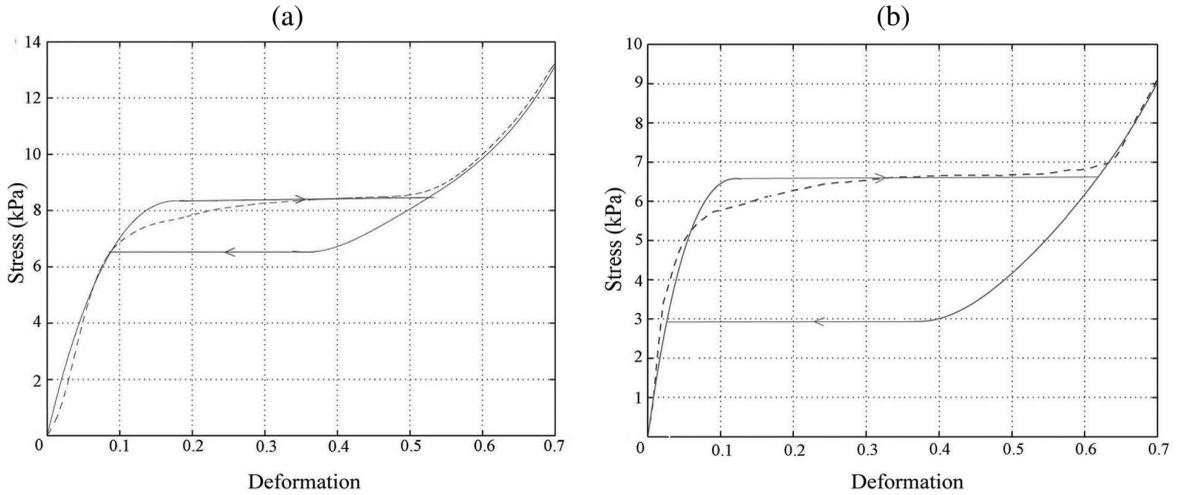
Figure 8. Theoretical response curves and hysteresis loop (solid lines), compared with average experimental response at loading (dotted line) for the 10 mm (a) specimens and the 50 mm (b) specimens.

following the first ascending branch of the response curve. Both correspond to a homogeneous configuration with all springs in phase A. A two-phase configuration with one spring more deformed than the others is shown in the third row, and the phase transitions of all springs, one after the other, are shown in the following rows. When all layers are strongly deformed as shown in the last row, the specimen is back to homogeneous deformation.

3.4. *Response at unloading.* At unloading, the model predicts a similar behavior: after reaching the force σ_{min}, the system approximately follows the horizontal line $\sigma = \sigma_{min}$, successively assuming configurations with m gradually increasing from zero to n. The hysteresis loop determined in this way has indeed been observed in experiments on polymer foams [Gong et al. 2005], on aluminium foams [Bart-Smith et al. 1998; Bastawros et al. 2000], and on shape memory alloys [Miyazaki and Otsuka 1989; Ortin 1992; Tanaka et al. 1996].

If the system is unloaded when $m > 0$, that is, when there are still springs in phase A, the system follows, backwards, the two-phase equilibrium curve for the given m until the value σ_{min} is attained. For further decreasing deformations, the system approximately follows the horizontal line $\sigma = \sigma_{min}$, until all springs go back to phase A. A comparison of this prediction with experiments made by the authors is given in the next section.

4. Comparison with experiment

In Figure 8, the model's response is compared with the experimental results for the 10 and the 50 mm specimens. As explained in Section 2.2, the two groups of specimens are characterized by different material constants. The dotted curves are the average experimental curves of Figure 3 and the solid lines are the response curves of the model, with the values of the constitutive constants reported in Table 1. In the latter, according to our model's prediction, the plateaus should indeed be wavy lines. But the waves have been neglected, supposing that the number of springs is conveniently large.
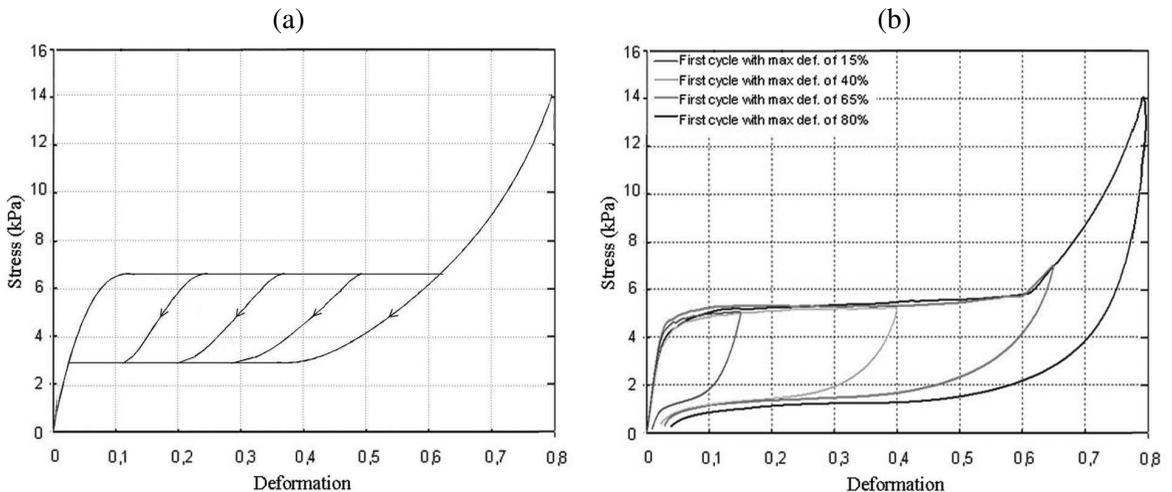
	10 mm specimens	*50 mm specimens*
α	4.2 kPa	2.92 kPa
μ	4.2 kPa	2.92 kPa
c	50.8 kPa	69.9 kPa
n	5	7
β	2.5 kPa	3.5 kPa
k	47	18
a	0.67	0.72

Table 1. Values of the constitutive constants.

The constants in Table 1 have been chosen for the best fitting of the experimental curves in the first loading branch, $\varepsilon_0 < 0.1$, and for elongations larger than $\varepsilon_0 > 0.3$. Indeed, our model does not predict the positive slope exhibited by the experimental curves in the range $0.1 < \varepsilon_0 < 0.3$. This part of the loading diagram has been studied in [Puglisi and Truskinovsky 2001; Marzano et al. 2003]. In [Puglisi and Truskinovsky 2001], curves with positive slope are obtained from chains made of springs with different energies.

Figure 9 compares the theoretical and experimental loading-unloading curves for 50 mm specimens, for different values of the maximum elongation $\varepsilon_{\max}$. The curves show a qualitative agreement in the shapes of the hysteresis loops. But there are also some discrepancies:

(i) In the model, all unloading curves begin at the upper plateau. In the experiments, the upper plateau ends at $\varepsilon_p \approx 60\,\%$, and yet the unloading curves for $\varepsilon_{\max} > 60\,\%$ do not follow backwards the unloading curve up to ε_p as predicted by the model.

(a)   (b)

Figure 9. Theoretical (a) and experimental (b) loading-unloading curves for the 50 mm specimens, showing the shapes of the hysteresis loops for different maximum elongations [Pampolini and Del Piero 2008].

(ii) In the model the lower plateau is horizontal, and it is the same for all $\varepsilon_{\max}$. In the experiments there are different lower plateaus for different $\varepsilon_{\max}$, and all have a variable positive slope. The transition from the descending curve to the plateau is not evident.

(iii) In the model, after a complete loading-unloading cycle, all curves end at the origin. In the experiments, there is a residual deformation whose amount increases with $\varepsilon_{\max}$.

It is possible to eliminate the discrepancies in point (ii) by introducing a damage variable (see [Pampolini and Del Piero 2008]), and to attribute those in point (iii) to residual plastic deformation. But both seem rather to be due to retarded elasticity, with a decay time much larger than the duration of the experiment. Indeed, our observations confirm those of [Gong et al. 2005], according to which the residual deformations are completely recovered when the specimen is left at rest for 48 hours.

References

[Bardenhagen et al. 2005] S. G. Bardenhagen, A. D. Brydon, and J. E. Guilkey, "Insight into the physics of foam densification via numerical simulation", *J. Mech. Phys. Solids* **53** (2005), 597–617.

[Bart-Smith et al. 1998] H. Bart-Smith, A.-F. Bastawros, D. R. Mumm, A. G. Evans, D. J. Sypeck, and H. N. G. Wadley, "Compressive deformation and yielding mechanisms in cellular Al alloys determined using X-ray tomography and surface strain mapping", *Acta Materialia* **46** (1998), 3583–3592.

[Bastawros et al. 2000] A.-F. Bastawros, H. Bart-Smith, and A. G. Evans, "Experimental analysis of deformation mechanism in a closed-cell aluminium alloy", *J. Mech. Phys. Solids* **48** (2000), 301–322.

[Del Piero and Truskinovsky ≥ 2008] G. Del Piero and L. Truskinovsky, "Elastic bars with decohesions". In preparation.

[Ericksen 1975] J. L. Ericksen, "Equilibrium of bars", *J. Elast.* **5** (1975), 191–201.

[Fedelich and Zanzotto 1992] B. Fedelich and G. Zanzotto, "Hysteresis in discrete systems of possibly interacting elements with a double-well energy", *J. Nonlinear Sci.* **2** (1992), 319–342.

[Froli and Royer-Carfagni 1997] M. Froli and G. F. Royer-Carfagni, "An experimental study of the Portevin -Le Chatelier effect in steel bars", in *Proc. 13th AIMETA National Congress of Theoretical and Applied Mechanics*, 1997.

[Froli and Royer-Carfagni 1999] M. Froli and G. F. Royer-Carfagni, "Discontinuous deformation of tensile steel bars: experimental results", *ASCE J. Engng Mech.* **12** (1999), 1243–1250.

[Gent and Thomas 1963] A. N. Gent and A. G. Thomas, "Mechanics of foamed elastic materials", *Rubber Chem. Technol* **36** (1963), 597–610.

[Gibson and Ashby 1997] L. J. Gibson and M. F. Ashby, *Cellular solids: structure and properties*, second ed., Cambridge University Press, 1997.

[Gioia et al. 2001] G. Gioia, Y. Wang, and A. M. Cuitinho, "The energetics of heterogeneous deformation in open-cell solid foams", *Proc. R. Soc. London A* **457** (2001), 1079–1096.

[Gong and Kyriakides 2007] L. Gong and S. Kyriakides, "On the crushing stress of open cell foams", *ASME J. Appl. Mechanics* **73** (2007), 807–814.

[Gong et al. 2005] L. Gong, S. Kyriakides, and W. Y. Jang, "Compressive response of open-cell foams. Part I: Morphology and elastic properties", *Int. J. Solids Struct.* **42** (2005), 1355–1379.

[Lakes et al. 1993] R. Lakes, P. Rosakis, and A. Ruina, "Microbuckling instability in elastomeric cellular solids", *J. Mater. Sci.* **28** (1993), 4667–4672.

[Marzano et al. 2003] S. Marzano, M. D. Piccioni, and G. Puglisi, "Un modello di isteresi per fili di leghe a memoria di forma", in *Proc. 16th AIMETA National Congress of Theoretical and Applied Mechanics*, 2003.

[Miyazaki and Otsuka 1989] S. Miyazaki and K. Otsuka, "Development of shape memory alloys", *ISIJ Int.* **29** (1989), 353–377.

[Müller and Villaggio 1977] I. Müller and P. Villaggio, "A model for an elastic-plastic body", *Arch. Ration. Mech. Anal.* **65** (1977), 25–46.

[Ogden 1997] R. W. Ogden, *Non-linear elastic deformations*, Dover Publications, New York, 1997.

[Ortin 1992] J. Ortin, "Preisach modeling of hysteresis for a pseudoelastic Cu-Zn-Al single crystal", *J. Appl. Phys.* **71** (1992), 1454–1461.

[Pampolini and Del Piero 2008] G. Pampolini and G. Del Piero, "Strain localization and cyclic damage of polyurethane foam cylinders: experimental tests and theoretical model", *Proc. AGS08, The Second Euro-Mediterranean Symposium on the Advances in Geomaterials and Structures, Hammamet* **1** (2008), 111–121.

[Puglisi and Truskinovsky 2000] G. Puglisi and L. Truskinovsky, "Mechanics of a discrete chain with bi-stable elements", *J. Mech. Phys. Solids* **48** (2000), 1–27.

[Puglisi and Truskinovsky 2001] G. Puglisi and L. Truskinovsky, "Hardening and hysteresis in transformational plasticity", in *Proc. 15th AIMETA National Congress of Theoretical and Applied Mechanics*, 2001.

[Tanaka et al. 1996] K. Tanaka, F. Nishimura, M. Matsui, H. Tobushi, and P.-H. Lin, "Phenomenological analysis of plateaus on stress-strain hysteresis in TiNi shape memory alloy wires", *Mechanics of Materials* **24** (1996), 19–30.

[Wang and Cuitinho 2002] Y. Wang and A. M. Cuitinho, "Full-field measurements of heterogeneous deformation patterns on polymeric foams using digital image correlation", *Int. J. Solids Struct.* **39** (2002), 3777–3796.

[Warren and Kraynik 1997] W. E. Warren and A. M. Kraynik, "Linear elastic behavior of a low-density Kelvin foam with open cells", *ASME J. Appl. Mech.* **64** (1997), 787–793.

GIAMPIERO PAMPOLINI: pampolini@lma.cnrs-mrs.fr
Laboratoire de Mécanique et d'Acoustique, 31 chemin Joseph-Aiguier, 13402 Marseille, France

GIANPIETRO DEL PIERO: dlpgpt@unife.it
Università di Ferrara, Via Saragat 1, 44100 Ferrara, Italy